Title
Exposure assessment of particulate matter air pollution before, during, and after the 2003 Southern California wildfires

Journal
Atmospheric Environment, 40(18)

ISSN
1352-2310

Authors
Wu, J
Winer, A M
Delfino, R J

Publication Date
2006-06-01

Peer reviewed

Exposure Assessment of Particulate Matter Air Pollution Before, During, and After the 2003 Southern California Wildfires

Jun Wu,[1 *] Arthur M Winer [1] and Ralph J Delfino[2]

[1] Department of Environmental Health Sciences, School of Public Health, University of California, Los Angeles, CA 90095-1772, USA

[2] Epidemiology Division, Department of Medicine, University of California, Irvine, CA 92617, USA

ATMOSPHERIC ENVIRONMENT

January 27, 2006

*Corresponding author. Environmental Health Sciences Department, Room CHS 56-070, School of Public Health, University of California, Los Angeles, CA 90095-1772. Tel: 310-825-3161, fax: 310-206-3358, email: junwu@ucla.edu

ABSTRACT

Exposure to biomass smoke has been associated with increased respiratory illness and symptoms. The goal of this study was to estimate daily particulate matter (PM; PM_{10} and $PM_{2.5}$) concentrations at a zip-code level for southern California before, during and after the 2003 southern California wildfires. On average, heavy smoke from the fires increased PM_{10} and $PM_{2.5}$ concentration by 160 and 100 $\mu g\ m^{-3}$, respectively. Missing PM concentrations from the every 3rd or 6th day routine measurements or due to the incapacitation of monitors and/or stations by the fires were estimated based on (1) temporal profiles of continuous TEOM or BAM data at co-located or closely-located sites; and (2) light extinction, meteorological conditions, and smoke information extracted from MODIS satellite images at a 250 m resolution. Light extinction coefficient, smoke, and relatively humidity were the most important factors strongly associated with PM concentrations, especially $PM_{2.5}$. Spatial interpolations of PM concentrations were performed using inverse distance weighting (IDW), kriging or cokriging methods for the non-fire periods. Kriging was not superior to IDW in many cases due to the small number of monitoring stations. Since the fire and smoke created highly heterogeneous pollution surfaces, typical IDW and kriging could not work during the fires. Polygons were created based on satellite images to represent each smoke-covered area under different smoke densities. Concentrations were assigned to each polygon using measured or valid estimated concentrations at the corresponding monitoring stations, or at other stations under similar smoke conditions. In summary, population-weighted PM_{10} and $PM_{2.5}$ concentrations were 190 and 90 $\mu g\ m^{-3}$, and 125 and 75 $\mu g\ m^{-3}$ under heavy and light smoke conditions, respectively, in contrast to concentrations of 40 and 20 $\mu g\ m^{-3}$ for PM_{10} and $PM_{2.5}$, respectively, during the non-fire periods. The methodology we developed in this study is also applicable to other regions to a greater or lesser extent based on the availability of satellite, visibility and air quality data.

Key Words

Particulate Matter; Satellite Image; Visibility; Smoke; Spatial Interpolation

1. Introduction

Catastrophic wildfires struck southern California in late October, 2003. Strong, dry winds from inland deserts fanned flames from as many as nine distinct fires from Ventura County in the north, to the U.S. Mexican border in the south. The fires burned nearly three-quarters of a million acres of land and destroyed approximately 5000 residences and outbuildings (California Air Resources Board, 2003). The wildfires generated large amounts of dense smoke that covered much of southern California for days.

Evaluation of the public health impacts is needed to inform the public in future fire events regarding health hazards and appropriate actions to reduce exposures. Particulate matter (PM) is the air pollutant with the greatest increase in concentrations during fire events (Phuleria et al., 2005), and biomass-related PM has been associated with a variety of adverse health outcomes, particularly respiratory morbidity (Brauer, 1999; Duclos et al., 1990; Kunii et al., 2002; Lipsett et al., 1997; Mott et al., 2002; Ostro et al., 1994; Robin, 1996). The PM concentration and composition may vary greatly during fire events. Studies have shown 24-hr average concentrations of particulate matter with an aerodynamic diameter of 10 μm (PM_{10}) ranged between 350 and 400 μg m^{-3} in the Megram and Onion Wildfires in northern California in the Fall of 1999, and hourly peak concentrations can be as high as 4000 μg m^{-3} (Herr, 2003). During fire periods in communities where wood burning was common, and in plumes associated with large-scale tropical forest fires, the average concentrations of particulate matter with an aerodynamic diameter of 2.5 μm ($PM_{2.5}$) were frequently 2-4 times and up to 15 times those of the background $PM_{2.5}$ concentrations (Brauer, 1999). An average increment of about 250 μg m^{-3} in $PM_{2.5}$ concentrations was observed from biomass burning in Palembang, Sumatra, Indonesia in the November 1997 wildfire (Pinto and Grant, 1999).

The large range of PM_{10} and $PM_{2.5}$ concentrations during fires makes it difficult for epidemiological studies to investigate public health impacts of PM air pollution from wildfires since many of these studies require temporally and spatially resolved exposure data, while only sporadic and widely spaced *in situ* measurements are available due to cost considerations. In the United States, most routine PM monitoring have been performed every 3rd or 6th day, rather than daily. Typically monitoring station networks are also limited spatially and are not uniformly distributed. For example, even though

southern California has one of the densest PM monitoring networks nationwide, in 2003 only 37 stations measured PM_{10} and/or $PM_{2.5}$ concentrations in the region of the South Coast and San Diego Air Basins, an area of over 27,000 km^2. This situation was worse during the severe 2003 wildfires when frequent invalid PM measurements occurred due to unusually heavy PM mass loadings or due to stations being incapacitated from direct fire damage.

Because of the temporal and spatial limitations in air quality measurements from ground monitoring stations, recent studies have begun to use satellite remote-sensing data to examine the impacts of specific fire events on regional and urban air quality. Satellite images have been used qualitatively to identify fire and dust events (Falke et al., 2001; Husar et al., 2001). The Moderate Resolution Imaging Spectroradiometer (MODIS) aerosol optical depth (AOD) data and the Geostationary Operational Environmental Satellite East (GOES) Aerosol and Smoke Product (GASP) have been used to evaluate particulate matter levels for specific events (Engel-Cox et al., 2004; Husar et al., 2001; Hutchinson, 2003; Wang and Christopher, 2003). The MODIS provides AOD data every day with a resolution of approximately 10 km (http://idea.ssec.wisc.edu), while the GOES GASP provides every half-hour AOD data at a four-kilometer resolution (http://www.ssd.noaa.gov/PS/FIRE/GASP/gasp.html). However, frequent missing AOD values were observed in both datasets over our study region during the fire period since the algorithm used to calculate the AOD data may mistake dense smoke for cloud and mask it from the AOD calculation, or eliminate these values during its screening process (Engel-Cox et al., 2004). In addition, correlations of MODIS aerosol optical depth with ground-based PM concentrations were found to be poor in the western US (e.g. AOD and $PM_{2.5}$ had a correlation coefficient of 0.13 for Los Angeles) (Engel-Cox et al., 2004). For these reasons, no AOD data were used in this study.

This manuscript describes the exposure assessment portion of a time series epidemiological study that investigates the impact of particulate matter from the 2003 southern California wildfires on hospital admission rates for various respiratory and cardiovascular illnesses at the zip-code level. The goal of this study was to estimate daily PM_{10} and $PM_{2.5}$ concentrations at the zip-code level in the South Coast Air Basin and San Diego Air Basin before (10/1/2003-10/20/2003), during (10/21/2003-10/29/2003),

and after (10/31/2003-11/15/2003) the 2003 southern California wildfires. We estimated PM_{10} and $PM_{2.5}$ mass concentrations between the 3rd and 6th -day sampling intervals using co-located real-time measurements, airport visibility observations, meteorological data, and smoke information from satellite images. Spatial interpolation of PM concentrations was performed using inverse distance weighting (IDW), kriging or cokriging methods for days in the non-fire periods. For days during the fire period, MODIS satellite images were used to identify each smoke-covered area, and PM concentrations were estimated for each smoke-covered region based on available air monitoring data, valid estimated concentrations, measured concentration under the same smoke coverage, or average increments of PM concentrations under different smoke densities during this wildfire season.

2. Methods

2.1. Method Overview

Two challenges were faced in this study to estimate daily PM concentrations at the zip-code level. First, most PM measurements at routine air quality monitoring stations in the U.S. were operated every 3rd or 6th day, leading to a significant number of days with missing PM data in our study period, especially during fire periods when PM monitors were also frequently disabled by high PM concentrations and air quality stations were incapacitated by direct fire damage. Second, fires produced a large range of PM concentrations and very heterogeneous pollution surfaces, which made normal spatial interpolation impossible. Many epidemiological studies have developed relatively standard procedures to fill missing data in the routinely collected ambient monitoring data, e.g. using measurements from co-located or close-located sites, or previous measurements, to assign temporal or spatial profiles. However, this was not applicable to the fire periods since wildfires are erratic events and concentrations at an in-smoke station can be much higher than those at a nearby station outside the smoke area. To account for the remarkable smoke impacts on PM concentrations at a fine spatial scale, we utilized various data sources other than PM measurements, including MODIS satellite images, visibility data, and meteorological data.

Figure 1 illustrates the overall methodology we used to estimate daily PM_{10} and $PM_{2.5}$ concentrations at zip-code centroids for the non-fire and fire periods. First, smoke information was extracted from MODIS satellite images at a 250 m resolution. Polygons were created to represent each smoke-covered area and were assigned different smoke density (0=no fire and smoke, 1=light smoke, 2=heavy smoke). The same smoke density code was also assigned to the corresponding PM monitoring stations.

Then, two types of regression equations were tested to fill in missing PM values, including the regression of filter PM data against real-time PM concentrations at co-located and close-located sites, and the regression of PM concentrations against smoke density, light extinction coefficient, and meteorological measurements at the same or nearby sites. Regression equations with R^2 equal or greater than 0.5 were selected to fill in missing PM values.

After the temporal missing data were filled as much as possible, spatial interpolation was conducted separately for the non-fire and the fire periods. For days before and after the fires, we applied IDW, kriging and co-kriging spatial interpolations, and selected the procedure that yielded a reasonable pollution surface and the least root mean square errors (RMSE). For days during the fires, measured or valid estimated concentrations at air quality stations were assigned to each corresponding smoke polygon. For smoke areas with no monitoring stations or no valid PM estimates, concentrations were estimated based on PM concentrations under similar smoke conditions. For areas under no smoke, random points were created to define the areas that were not directly impacted by any smoke, and IDW was applied to create pollution surfaces. Finally, daily PM_{10} and $PM_{2.5}$ concentrations were assigned to each zip-code centroid in our study region based on the pollution surface maps.

2.2. Data Sources

We downloaded the MODIS satellite images from the gallery of NASA's MODIS Rapid Response System (http://rapidfire.sci.gsfc.nasa.gov/gallery), which provided true-color 250-m resolution images of southern California for most of the fire days (10/21 to 10/23 and 10/25 to 10/29, 2003) during our study period. The Terra and Aqua satellites pass southern California in the late morning and early afternoon, respectively, with an approximately three-hour difference. For each fire day, we chose either a Terra or an

Aqua satellite image with the best coverage and quality. For the fire days with no images provided by the gallery (10/24/2003), we obtained MOD02 data from NASA's Distributed Active Archive Center (DAAC) (http://daac.gsfc.nasa.gov/daac-bin/MODIS/Data_order.pl?PRINT=1), and converted them to 250-m resolution images using procedures described by Gumley et al. (2003).

Continuous and filter-based $PM_{2.5}$ and PM_{10} data were obtained from the California Air Resources Board, the South Coast Air Quality Management District (SCAQMD), and the San Diego Air Pollution Control District for the California South Coast Air Basin (SoCAB) and for the San Diego Basin (SDB) during August-December, 2003. Although the health outcome analysis will be focused on the period of October 1 to November 15, 2003, we included data from August 1 to December 31, 2003 in the exposure assessment, which provided data more representative of the non-fire periods. Hourly PM concentrations were measured by Taper Element Oscillating Microbalance (TEOM) and Beta Attenuation Monitor (BAM) instruments, while daily, every 3rd day, and every 6th day data were measured by the Federal Reference Method (FRM) Sampler for $PM_{2.5}$ and the size-selective inlet high-volume sampler (SSI) for PM_{10} (also an FRM). Wind speed, wind direction, temperature, and relatively humidity were also obtained for most air quality stations.

Meteorological data measured by the Automated Surface Observing System (ASOS) were obtained from the National Climatic Data Center (NCDC) for the study region during August to December, 2003. The data included hourly visibility, temperature, wind speed, wind direction, relative humidity, and precipitation measurements. The visibility data were archived in 18 distinct visual range bins: <1/4, 1/4, 1/2, 3/4, 1 1/4, 1 1/2, 1 3/4, 2, 2 1/2, 3, 4, 5, 6, 7, 8, 9, and 10+ miles.

In total, there were 37 air quality and 20 ASOS weather stations in the study region. Figure 2 shows air quality and ASOS stations overlaid with the MODIS satellite image on 10/25/2003. The SoCAB contained one BAM, nine TEOM, and fifteen SSI samplers for PM_{10}, and four BAM and seventeen FRM samplers for $PM_{2.5}$, respectively. The SDB had one TEOM and six SSI samplers for PM_{10}, and two BAM and five FRM samplers for $PM_{2.5}$, respectively. Most of the PM_{10} SSI samplers measured every 6th day, while about half of the $PM_{2.5}$ FRM samplers operated every 3rd day.

2.3. Data Pre-Processing

2.3.1 Satellite Data

All satellite images were geo-referenced and imported onto the GIS platform. ArcGIS 9.0 software (ESRI^{TM}) was used to identify and manually geo-locate the fires and extent of the plumes on the map. We used three categories, 0 (no fire and smoke), 1 (light smoke), and 2 (heavy smoke), to distinguish the status of fire and smoke at any location in the study region. The smoke was easy to identify if it was in close proximity to a fire. However, sometimes the smoke plume could not easily be distinguished from clouds or haze. This occurred for the satellite image at the end of the fire season on 10/29 due to the heavy cloud cover that day. In this case, the following two rules were applied to assign smoke events: 1) if the suspected cloud/smoke was connected with a fire, then it was identified as smoke; 2) if the PM concentrations at the monitoring stations covered by the cloud/smoke were unusually high, we assumed this site and the area were affected by smoke.

Although more categories are desirable to characterize smoke densities, we only used three categories that can be easily distinguished under visual inspection. More refined classifications might introduce exposure misclassification because of reduced statistical power to predict more than three levels. In addition, PM measurements were extremely limited during the fire period, especially for stations under smoke, which made it hard to obtain appropriate concentration estimates for additional smoke categories.

2.3.2 Air Quality Data

The reliability and consistency of all the air quality data were examined and apparent erroneous measurement data were excluded, e.g. those with error flags, as well as continuous measurements with constant values over a long time. The minimum, maximum, and mean concentrations of PM under different smoke conditions were calculated for each site. These results were used to examine the scale of the wildfire impact, to identify unusual events irrelevant to the wildfires, and to exclude erroneous measurement data. For example, PM_{10} concentrations at San Diego were unexpectedly high on 11/23/2003, three weeks after the fires (280 $\mu g\ m^{-3}$ compared to a maximum

concentration of 80 μg m^{-3} during the non-fire periods). Satellite images showed a strong Santa Ana wind carrying ash plumes from inland burn areas to the coastal areas of San Diego on that day, which caused the high PM_{10} concentrations. Therefore, we excluded the San Diego PM_{10} data on 11/23 from further analyses. $PM_{2.5}$ concentrations were not affected on that day.

2.4. Filling Missing Filter-Based Air Quality Data

In this study, thirteen out of fifteen PM_{10} SSI sites were operated every 6^{th} day, while eleven out of seventeen $PM_{2.5}$ FRM sites were operated every 3^{rd} or 6^{th} day. Since the filter-based measurements (SSI sampler for PM_{10} and the FRM sampler for $PM_{2.5}$) were FRM methods, and a majority of the air monitoring sites conducted only filter-based measurements, we conducted all the exposure estimates based on filter measurements or equivalent filter data.

2.4.1 Filling Missing Data Using Real-Time PM Measurements

Linear regression equations (Filter-based PM concentration = a + b*real-time PM concentrations) were conducted for filter-based measurements with TEOM or BAM data at six co-located stations, and at other nearby stations within a 33 km radius. Since smoke events increased PM concentrations significantly, we excluded the days when the filter sites had different smoke status than the TEOM or BAM sites, e.g. when one was covered by smoke while the other was not. Appropriate equations with R^2 greater than or equal to 0.5 were selected to fill missing data

2.4.2 Filling Missing Filter-Based Data Using Visibility, Smoke, and Other Meteorology Variables

Daily average meteorology parameters were calculated as median hourly values. The wind directions from 0 to 360 degrees were converted to a continuous integer variable with eight ordered values from 1 to 8 (Delfino et al., 1994). The highest value, 8, was assigned to the predominate wind direction, with values 7 to 1 assigned in descending order for less frequent directions. Visibility data were converted to light extinction coefficient (B_{ext}) based on a modified Koschmieder formula (Abbey et al., 1995). The extinction coefficient in 10 km^{-1} units is given by $B_{ext}\_C = 18.7\ C/Visibility$,

in which C represents a correction factor for relative humidity. However, previous work showed the RH-corrected light scattering coefficient did not help in predicting PM concentrations any better than uncorrected data (Alcorn et al., 2003). Therefore, we included both RH-corrected and uncorrected light extinction coefficients (B_{ext}_C and B_{ext}) in our analysis.

Thirty-two pairs of air quality and ASOS stations were identified within a 20 km radius. PM concentrations were then regressed against the smoke density and all meteorology variables at the air monitoring station and/or an adjacent ASOS station. For each site a two-variable linear regression equation (PM concentration = Intercept + ax*Variable1 + bx*Variable2) was selected with the highest R^2 equal or greater than 0.5. Variable1 and Variable2 were any combination of the smoke and meteorological variables that produced the highest R^2 for PM_{10} or $PM_{2.5}$ at a particular site. The inclusion of smoke information was helpful for predicting smoke impact, but may have introduced bias when predicting PM concentrations for non-fire days at sites that were strongly affected by smoke during the fires but exhibited relatively clean air during non-fire periods. Therefore, we also conducted regressions for the non-fire periods for smoke-affected sites after removing the smoke variable.

Negative or extremely high concentration estimates might occur using regression equations since input parameters on the prediction day might not satisfy the range of the parameters used to derive the equations. To reduce erroneous estimation results, we set a lower and upper bound for PM concentration predictions during the non-fire periods, using the minimum and maximum concentrations from measurement data during the same periods. During the fire period, threshold concentrations of 400 and 240 $\mu g\ m^{-3}$ were set for the PM_{10} and $PM_{2.5}$ concentrations, respectively, corresponding to the maximum PM_{10} and $PM_{2.5}$ concentrations of 375 $\mu g\ m^{-3}$ (PM_{10} TEOM at Upland, Los Angeles on 10/26), and 240 $\mu g\ m^{-3}$ ($PM_{2.5}$ at Chula Vista, San Diego on 10/27). These values were derived from available measurement data, which might underestimate PM concentrations in areas most strongly impacted by heavy smoke.

2.4.3 Modeled PM Concentrations at Stations under Smoke

As discussed in the Introduction and shown in the Results section, wildfires are associated with strong increases in PM concentrations, with a wide range varying by site and day, indicating the difficulty in predicting PM concentrations in smoke-affected areas. The regression equations ($R^2 \geq 0.5$) we obtained were derived from extremely limited data, in which no more than two (sometimes zero) PM measurements were available for a majority of sites during smoke impacts, indicating great uncertainties when these equations were used to predict in-smoke PM concentrations. Therefore, we treated the model-estimated concentrations only as reference values for stations under smoke. Each estimated concentration was compared with the measured concentration at nearby sites under the same smoke or similar smoke conditions. If a predicted value was comparable to the measured concentrations (within ±30%), it was labeled "valid" and kept for further analyses; otherwise, it was labeled "invalid" and PM concentrations at this site were re-estimated based on the following order: (1) $PM_{2.5}$/ PM_{10} ratios calculated from concurrent filter measurements at in-smoke sites, and $PM_{2.5}$ (for PM_{10} estimation) or PM_{10} (for $PM_{2.5}$ estimation) concentrations measured at the same or nearby station if possible; (2) PM measurements at stations under similar smoke coverage; or (3) the averaged concentrations under light and heavy smoke conditions.

2.5. Spatial Interpolation of PM Concentrations

2.5.1 Non-fire periods

The Geostatistical Analyst extension from ESRI™ was used to interpolate the processed air quality data from scattered monitoring stations to about 560 unique zip codes for the non-fire periods. We employed two commonly-used weighted average interpolation methods, inverse distance weighting and kriging, to create pollution surfaces from limited data at stations. We also explored the cokriging process by utilizing several secondary variables, including $PM_{2.5}$ (when predicting PM_{10}), PM_{10} (when predicting $PM_{2.5}$), B_{ext}, wind speed, wind direction, and temperature.

We compared the pollution surfaces created from the IDW, kriging and cokriging interpolation methods. A map was selected for each pollutant-day by visually examining the pollution surface and comparing the root mean square errors. Visual examination was

conducted to exclude maps that did not follow any distribution patterns, or had a wrong distribution pattern. For example, typically $PM_{2.5}$ concentrations in the SoCAB increased from the coast to inland areas (due to secondary particle formation), reached the highest value around Riverside, and dropped at areas further inland. A map was assumed unreasonable if it apparently contradicted the general distribution patterns. Among all reasonable maps, the map with the lowest RMSE was selected for the final exposure estimation at zip-code centroids.

2.5.2 Fire Period

IDW or ordinary kriging were not sufficient to reconstruct pollution surfaces when the region was strongly affected by smoke plumes since data from the relative widely spaced monitoring stations could not adequately characterize capture the smoke-affected areas. In this study, various polygons were created based on satellite images to represent areas covered by light and heavy smoke, respectively. If a polygon covered more than one air quality station with measured or valid estimated concentrations, the polygon was sub-divided into smaller areas until each polygon contained no more than one station. A valid concentration from the corresponding air monitoring station was assigned to each polygon if possible. If a smoke-covered area contained no monitoring station, concentrations were assigned based on $PM_{2.5}$ (for PM_{10} estimation) or PM_{10} (for $PM_{2.5}$ estimation) concentrations measured at the nearby stations under similar smoke coverage, or simply the averaged concentrations under the light and heavy smoke conditions.

After PM concentrations were assigned to all smoke-covered areas, random points were generated at the outside edge of smoke plumes to define the areas that were not directly impacted by smoke. Concentrations were assigned to these random points based on measured concentrations at nearby sites outside the smoke area, the concentrations inside the smoke area, and the relative distance of the point to the nearby site and to the smoke. Then, the IDW method was used to create pollution surfaces for non-smoke areas, using all measured, estimated, and random data points outside the smoke regions. Finally, we overlaid the PM concentration surface for smoke-covered areas with the surface for non-smoke areas to produce a final map that was used to estimate zip-code centroid concentrations during the fire period.

3. Results

3.1. Smoke Impact

The highest 24-hr concentrations from filter-based measurements were 270 μg m^{-3} for PM_{10} at North Long Beach, Los Angeles on 10/26/2003, and 240 μg m^{-3} for $PM_{2.5}$ at Chula Vista, San Diego on 10/27/2003. The maximum daily-averaged concentrations of PM_{10} and $PM_{2.5}$ from real-time measurements were 375 μg m^{-3} (TEOM data) at Upland, Los Angeles on 10/26/2003, and 270 μg m^{-3} (BAM data) at Escondido, San Diego on 10/28/2003, respectively.

Figure 3 shows the average PM concentrations (filter measurements) under different smoke scenarios. The average PM_{10} and $PM_{2.5}$ concentrations under light smoke and heavy smoke were 122 and 69 μg m^{-3}, and 200 and 117 μg m^{-3}, respectively. Compared to measurements during the non-fire periods, light smoke increased PM_{10} and $PM_{2.5}$ concentrations by about 80 and 50 μg m^{-3}, respectively, while heavy smoke increased PM_{10} and $PM_{2.5}$ concentrations by about 160 and 100 μg m^{-3}, respectively. There was substantial site-to-site variation in the range of increase. Real-time PM_{10} TEOM measurement at five additional sites (data not shown) showed similar results of about 80 μg m^{-3} increase for light smoke (at five sites) and 180 μg m^{-3} increase for heavy smoke (at four sites). Real-time $PM_{2.5}$ BAM data at three additional sites (data not shown) showed about a 50 μg m^{-3} increase for light smoke (at two sites) and 90 μg m^{-3} increase for heavy smoke (at one site).

The PM concentrations before and after the wildfires were comparable, with slightly higher concentrations before the fires. The average PM concentrations under no smoke condition during the fire period increased about 60% (69 vs. 42 μg m^{-3} for PM_{10} and 31 vs. 19 μg m^{-3} for $PM_{2.5}$) compared with those measured during the non-fire periods. This indicates that, as expected, fires increased background PM concentrations significantly, which could not be captured by satellite images. Another possible reason is that since the wildfire occurred during a Santa Ana period of hot dry winds coming out of the deserts, PM concentrations could have been higher due to high temperatures and resuspended dust.

3.2. Regression Results Using Real-Time PM Data

The regression equations for filter-based data against TEOM or BAM measurements at co-located sites are shown in Table 1. All p-values for the slope were less than 0.0001. Significant non-zero intercepts were observed at all five stations with co-located BAM and filter instruments, which indicated systematic bias from the BAM instrument, at least at the selected sites and during the study period. The four regression equations against $PM_{2.5}$ BAM data yielded slopes from 0.48 to 0.85, indicating the BAM instrument over-estimated $PM_{2.5}$ concentrations compared to the filter-based method. However, a higher than unit slope (Slope=1.5; R^2=0.94; N=19) was observed for regression of PM_{10} filter data against BAM data at the Los Angeles-North Main Street station. The high R^2 and a side-by-side plot showed this filter data correlated well with BAM measurements. Therefore, this equation was still used to fill missing filter data at this site although we could not find a plausible explanation for the underestimation of PM_{10} concentrations from the BAM. Regression equations against TEOM PM_{10} data had slopes of 1.03, 1.09 and 1.35, indicating lower values from TEOM measurements than filter-based measurements. This is expected since TEOM instruments are operated at elevated temperature to avoid problems with water collecting, which results in the volatilization of ammonium nitrate and organic species (Chung et al., 2001).

Regression equations were also obtained at six PM_{10} and nine $PM_{2.5}$ stations for filter-based data against TEOM or BAM measurements at nearby stations ($R^2 \geq 0.5$) within a 33 km radius (data not shown). The regression equations of filter-based PM_{10} and TEOM data at nearby sites had slopes ranging from 0.66 to 1.61 and R^2 from 0.55 to 0.79, while the regression equations of filter-based $PM_{2.5}$ and BAM data at nearby sites had slopes ranging from 0.48 to 0.81 and R^2 from 0.53 to 0.91. All p-values for the slope were less than 0.0001. Better correlations were observed for $PM_{2.5}$ than PM_{10} data, indicating PM_{10} concentrations might be impacted more by local sources than $PM_{2.5}$.

3.3. Regression Results Using Visibility, Meteorology, and Smoke Information

Table 2 lists fifteen and fourteen-selected regression equations for PM_{10} and $PM_{2.5}$, respectively, with R^2 equal or greater than 0.5. The PM_{10} regression equations showed more complex patterns than those for $PM_{2.5}$. Among the fifteen PM_{10} regression

equations, eleven had B_{ext} as a significant variable, and six had smoke as a significant second variable. Relative humidity, temperature, and wind speed also appeared as a predictor variable for a few models. Uncorrected B_{ext} outperformed RH-corrected B_{ext}_C in seven out of the eleven cases. The slope of the B_{ext} variable ranged from 3 to 70, with an average of 18, indicating that a unit increment in the B_{ext} corresponded to an average increase of 18 $\mu g\ m^{-3}$ in PM_{10} concentrations. The slope of the smoke variable ranged from 50 to 115, with an average of 75, indicating an average light and heavy smoke impact of 75 $\mu g\ m^{-3}$ and 150 $\mu g\ m^{-3}$, respectively. The estimated smoke impact was comparable to the value obtained from Figure 3. Relative humidity was negatively associated with PM_{10} concentrations in four of the regression equations, with a slope ranging from -0.72 to -1.26.

$PM_{2.5}$ regression equations had an R^2 ranging from 0.6 to 0.98, with B_{ext} as a significant parameter (p-value <0.0001) in all equations. Smoke (at ten stations), wind speed (at two stations), and temperature (at two stations) appeared to be significant second variables in the regression models. The $PM_{2.5}$ concentrations had a positive correlation with the B_{ext} variable, with an average slope of 8 (range from 5 to 12), indicating that on average a unit increment in B_{ext} corresponded to an 8 $\mu g\ m^{-3}$ increase in $PM_{2.5}$ concentrations. The smoke variable had an average slope of 40 (range from 7 to 100), comparable to our previous results that light smoke increased $PM_{2.5}$ concentrations by 50 $\mu g\ m^{-3}$.

We examined the difference in regression equations using all the data vs. using data from non-fire periods, and found that although the smoke variable significantly increased R^2, the slope difference for the common variables other than smoke was small for many comparable cases, indicating these variables were also important predictors in addition to the smoke variable. Therefore, no modifications to models were conducted to most of the estimated PM concentrations during the non-fire periods.

We note regression equations we developed were site-specific since the sites were scattered over a large region, had varied meteorological parameters, and were influenced by different emission sources. In addition, not every station contained a full set of smoke, B_{ext} and meteorological variables used in the regression equations. For example, no PM_{10} measurements were available at any of the stations in San Diego during the fires,

leaving no smoke variable in the PM_{10} regression equations at these stations. Therefore, caution was needed when using these equations to estimate PM_{10} concentrations during the fires. Nevertheless, the equations we derived are still helpful for other studies since they revealed the important parameters and their relative impact on PM concentrations.

After applying all the appropriate regression equations as described above to predict PM concentrations at the air monitoring stations, we created a pollutant concentration matrix for each day in the study periods. The number of valid PM station measurements ranged from 14 to 22 in the study region during the non-fire periods. As noted earlier, the number of valid data points was smaller during the fire period due to a significant number of invalid PM estimates at stations under smoke.

3.4. Pollution Interpolation

3.4.1 Non-Fire Periods

Kriging demonstrated better performance than IDW in certain, but not all, cases, and both methods showed comparable results in a majority of cases. Kriging produced lower RSME in a number of cases. However, visual inspections found the results not reasonable in some cases because although we tried to fill missing data as much as possible, the number of valid data points on a single day, from 14 to 22, was still far from the density of points needed to produce reliable kriging results. In addition, although PM_{10} and $PM_{2.5}$ behaved more like regional pollutants, significant contributions from local sources were observed, which made kriging results problematic in some cases.

In general, PM_{10} results showed much higher root-mean-square errors than $PM_{2.5}$ data in both the IDW and kriging processes, partly because PM_{10} concentrations were about twice the $PM_{2.5}$ concentrations and partly because PM_{10} data had more heterogeneous distributions than the $PM_{2.5}$ data due to influences from local emissions. Therefore, kriging exhibited better performance in the interpolation of $PM_{2.5}$ data than of PM_{10} data.

Although including $PM_{2.5}$ as a secondary variable in the cokriging process improved the prediction of the PM_{10} pollution in a few cases, we found cokriging with meteorological parameters such as visibility, wind speed, wind direction, temperature etc. did not show much improvement over kriging in most cases. A possible reason is that we

already used substantial meteorology data in the regression to fill missing values in the air quality data. Therefore, not much additional value was added by including the meteorological parameters in the cokriging process. In addition, there were not enough closely-located pairs of ASOS and air monitoring stations.

For the final results, we chose either IDW, krigging or cokriging, whichever yielded a reasonable pollution surface and the least RMSE. Figure 4 shows an example of the $PM_{2.5}$ pollution surface created by IDW and kriging on 10/2/2003, where PM data from 19 monitoring stations were used in the interpolation. The root-mean-square values for IDW and kriging were 5.1 and 4.5, respectively, with the kriging creating a smoother surface.

3.4.2 Fire Period

Figure 5a shows an example of how we estimated PM concentrations in smoke-covered areas on 10/27/2003. Eleven polygons were created to cover the smoke region under different smoke densities; each polygon covered at most one monitoring station. As we indicated earlier, certain regression equations might not appropriately predict pollutant concentrations at stations under smoke due to insufficient in-smoke measurements. In this case, no PM_{10} measurements were available for all the San Diego stations during the fires. Modeled PM_{10} concentrations at the San Diego stations under heavy smoke ranged from 94 to 139 $\mu g\ m^{-3}$, which were apparently underestimates since available $PM_{2.5}$ measurements in this region were 170 to 240 $\mu g\ m^{-3}$ on the same day.

$PM_{2.5}/PM_{10}$ ratios were used as the first choice to re-estimate the invalid PM_{10} concentration at San Diego. The $PM_{2.5}/PM_{10}$ ratios in this study ranged from 0.11 to 1 (median=0.4; N=318) at sites during the non-fire periods, and from 0.19 to 0.88 (median=0.6; N=15) at in-smoke sites, which were lower than the ratio of 0.9 in biomass smoke reported by Ward and Hardy in 1991. The lower-than-expected $PM_{2.5}/PM_{10}$ ratios during the fire period were probably due to two reasons. First, the strong Santa Ana winds were expected to transport high concentrations of entrained ash (in coarse mode) and dust to the downwind areas. Second, rather than measuring PM concentrations directly from the fire, we obtained measurement data from existing air quality stations, most of which were far away from the fires and were affected by other emission sources

as well. For the San Diego stations on 10/27, we used a $PM_{2.5}/PM_{10}$ ratio of 0.8 (corresponding to $PM_{2.5}$ and PM_{10} concentrations of 210 and 300 $\mu g\ m^{-3}$, respectively) since these stations were relatively close to the fires and were strongly affected by direct smoke emissions.

IDW was used to create a pollution surface outside the smoke region, using measured and estimated concentrations at stations under no smoke, and estimated concentrations at random points adjacent to the smoke. The pollution surface for the smoke-covered area and the non-smoke areas were overlaid and appropriate PM concentrations were spatially allocated to each zip-code centroid over the region. Figure 5b shows the interpolated PM_{10} concentrations at zip-code centroids over the study region on 10/27/2003. The PM_{10} concentrations ranged from about 30 to 300 $\mu g\ m^{-3}$, with the highest occurring for heavy smoke in south San Diego. Similar procedures were conducted for the other days as we demonstrated for the PM_{10} concentration on 10/27/2003.

3.5. Population-Weighted Concentrations

The study region had a population of 17.4 million people and 566 unique zip-codes (Census 2000). During the 2003 wildfire period (10/21/2003-10/29/2003), 94%, 59%, and 10% of zip-codes (corresponding to 16.5 million, 10.7 million, and 1.7 million populations, respectively) in the region were covered by light or heavy smoke for at least one, two, or five days, respectively. The population-weighted PM_{10} and $PM_{2.5}$ concentrations were 190 and 90 $\mu g\ m^{-3}$, and 125 and 75 $\mu g\ m^{-3}$ under heavy and light smoke conditions, respectively, in contrast to concentrations of 40 and 20 $\mu g\ m^{-3}$ for PM_{10} and $PM_{2.5}$, respectively, during the non-fire period. The population-weighted PM_{10} and $PM_{2.5}$ concentrations were slightly lower than the measured concentrations under the same smoke conditions (Figure 3) since the wildfires normally developed from rural, less populated areas. However, our results still show the study region population was heavily impacted by smoke from wildfires.

4. Discussion

Satellite images were essential in this study to provide smoke coverage and smoke density information over the region, which was important in estimating PM concentrations at air monitoring stations during the fire period, and in spatially assigning PM concentrations for smoke-covered areas. Real-time or hourly satellite images would be ideal for this application, but the current once-a-day snapshots from satellite images were still useful in defining the smoke-affected areas and examining smoke densities. We explored the possibility of using AOD data in this analysis, but found too many missing values during the fire period over the study region. Therefore, no AOD data were used in this analysis; but they can be useful in future studies if better algorithms are developed to distinguish smoke from clouds and for studies where smoke is not too dense.

Although satellite images and AOD data are critical in estimating PM concentrations during fire seasons, they only provide one-dimensional information and are limited in describing vertical smoke distributions. This likely explains the significant site-to-site variations of smoke impact since we could not distinguish smoke near the ground versus aloft. It is difficult to estimate appropriately ground-level PM concentrations without additional information on the vertical smoke profiles. Lidar (light detection and ranging) systems can provide dynamic vertical information about smoke, cloud, and optical properties of the atmosphere (Ferrare et al., 2001; Voss et al., 2001), and thus hold promise for future research on wildfire impacts on air pollution. However, current Lidar technologies are aimed at the development of new instruments, and the applications are limited only to specific studies rather than routine monitoring. Therefore, no Lidar data were available for use in this study.

Significant differences occur among different PM instruments, e.g. filter-based vs. TEOM and BAM samplers. Measurements from different instruments should be converted to a single standard if possible. However, such conversions are usually site-specific based on the composition of the particulate matter, and sometimes no appropriate conversions can be conducted for certain sites and instruments. Using direct PM measurements from different instruments may be problematic for exposure estimates during non-fire periods when PM concentrations are relatively low and instrumental differences may be significant. However, instrumental differences may become trivial

during fire periods when PM concentrations can be up to ten times the concentrations during the non-fire season. Therefore, given extremely limited gravimetric measurement data during the fires, measured data from real-time instruments can be used directly to predict PM concentrations at stations under heavy smoke.

In this study, every 3rd or 6th day routine gravimetric PM measurements were filled based on continuous TEOM or BAM data at co-located or closely-located sites, as well as light extinction coefficient, meteorological parameters, and smoke information. As expected, light extinction coefficient and smoke were the two most important variables in predicting PM concentrations. The other meteorological variables were also shown to be significant in a small number of cases. Although we have used the criteria of R^2 greater than or equal to 0.5 to select regression equations, predicted PM concentrations could be far off the true values under certain conditions, especially for smoke impacted stations since smoke impacts were dramatic, non-linear, and complex. For example, the PM_{10} concentration at north Long Beach was 49 $\mu g\ m^{-3}$ on 10/25 (no smoke), but soared up to 269 $\mu g\ m^{-3}$ on 10/26 (heavy smoke), followed by 173 $\mu g\ m^{-3}$ on 10/27 (light smoke), and 107 $\mu g\ m^{-3}$ on 10/28 (light smoke). Therefore, careful inspections are needed of the predicted PM concentrations during the fire period, as we have shown in this study.

Many studies have compared IDW and kriging methods in spatial interpolation, not only in the air pollution field but also in other fields such as meteorology and geology. In some cases, the performance of kriging was better than IDW (Kravchenko and Bullock, 1999; Zimmerman et al., 1999). In other studies, IDW out performed kriging (Nalder and Wein, 1998; Weber and Englund, 1992). Other results have been mixed (Lapen and Hayhoe, 2003; Mueller et al., 2004). It is generally believed the performance of kriging improves relative to IDW as sampling density increases. Due to the limited density of monitoring stations, we did not find much improvement from kriging and cokriging over IDW, indicating the simple IDW method can be used as the first choice to predict PM concentrations during non-fire periods or for non-smoke regions when not enough measurement data are available. Due to the high heterogeneity of pollution surfaces from smoke impacts, IDW and kriging methods cannot be used directly in the spatial interpolation for fire-days, which need to be studied on a case-by-case basis.

In this study, PM concentrations were estimated based on smoke information from satellite images, measured PM data at air monitoring stations, and visibility data at ASOS stations. Although southern California has a relatively dense routine PM monitoring network compared to the rest of the U.S. and other countries, PM measurements were still extremely limited during the fire period due to the infrequent monitoring schedule for PM and the incapacitation of monitors and/or stations by the fires. The San Diego region had no PM_{10} measurements during the fires, which was similar to rural or urban areas where no monitoring data were available. In this case, satellite images (and possibly other satellite products like AOD data) and visibility data from airports or other weather stations were demonstrated to be useful in estimating PM concentrations. For rural areas where both PM and light scattering measurements are rare, satellite products can provide the density and spatial coverage of smoke almost anywhere on the earth, from which a rough estimation of PM concentrations can be obtained. Therefore, the methodology we described in this study is also applicable to other regions with less dense air quality monitoring networks or light scattering measurements.

5. Conclusion

This study estimated daily PM_{10} and $PM_{2.5}$ concentrations at a zip-code level for southern California before, during and after the 2003 southern California wildfires. To our knowledge, this is the first study that has systematically examined and estimated daily PM_{10} and $PM_{2.5}$ concentrations at such a fine spatial resolution over a relatively large study domain for this type of application.

We have successfully filled the missing data in the routine every 3^{rd} or 6^{th} day gravimetric PM measurements using temporal profiles of continuous TEOM or BAM data at co-located or closely-located sites, as well as light extinction, relevant meteorological parameters, and smoke information extracted from MODIS satellite images at a 250 m resolution. Light extinction coefficient and smoke were the two most important factors in predicting PM concentrations, especially $PM_{2.5}$. Among selected equations for $PM_{2.5}$ against light extinction coefficient and smoke, R^2 ranged from 0.64 to 0.98, by AQ site, with a median of 0.82.

During the fire period, smoke events dramatically increased local PM concentrations and created highly heterogeneous pollution surfaces. On average, heavy smoke increased PM_{10} and $PM_{2.5}$ concentrations by 160 and 100 $\mu g\ m^{-3}$, respectively. Since the fire and smoke created highly heterogeneous pollution surfaces, typical IDW and kriging could not work during the fires. Polygons were created based on satellite images to represent each smoke-covered area under different smoke densities. Concentrations in each smoke-polygon were assigned separately, using measured or valid estimated concentrations at the corresponding monitoring stations, or at other stations under similar smoke conditions. For the non-fire periods, spatial interpolations of PM concentrations were performed using inverse distance weighting, kriging or cokriging methods. Kriging improved the interpolation slightly in certain, but not all, cases. The overall population-weighted PM_{10} and $PM_{2.5}$ concentrations were 190 and 90 $\mu g\ m^{-3}$, and 125 and 75 $\mu g\ m^{-3}$, under heavy and light smoke conditions, respectively, during the 2003 southern California wildfires.

We conclude that the fine temporal-spatial resolution of the PM data generated from this project is suitable for linkage to the residential zip code of subjects admitted to hospital for cardiorespiratory illnesses. The methodology we developed in this study is also applicable to other regions to a greater or lesser extent based on the availability of satellite, visibility and air quality data.

Acknowledgements

This work was supported by the California South Coast Air Quality Management District (SCAQMD; Contract No. 04182). The contents of this paper and the findings of its authors do not necessarily reflect the views of the SCAQMD which has not approved or disapproved this report. The mention of trade names or commercial products does not constitute an endorsement or a recommendation of use.

References

Abbey, D.E., Ostro, B.E., Fraser, G., Vancuren, T., Burchette, R.J., 1995. Estimating fine particulates less than 2.5 microns in aerodynamic diameter ($PM_{2.5}$) from airport

visibility data in California. Journal of Exposure Analysis and Environmental Epidemiology 5, 161-80.

Alcorn, S.H., Prouty, J.D., Knoderer, C.A., Dye, T.S., Richards, L.W., 2003. Automated Surface Observing Systems. Section 2: Data Collections and Processing Methods Applied to 1-Minute ASOS Data. Report prepared for the Center for Air Pollution Impact and Trend Analysis, Washington University, STI-902180-2434b.

Brauer, M., 1999. Health Impacts of Biomass Air Pollution. In: Health Guidelines for Vegetation Fire Events - WHO/UNEP/WMO Background Papers pp. 186-257. World Health Organization.

California Air Resources Board, Air Quality and the Wildland Fires of Southern California, October, 2003. Available at http://arb.ca.gov/qaweb/ertoutside/socalfires/. Accessed on April 13, 2005.

Chung, A., Chang, D.P.Y., Kleeman, M.J., Kerry, D.P., Cahill, T.A., Dutcher, D., McDougall, E.M., Stroud, K., 2001. Comparison of real-time instruments used to monitor airborne particulate matter. Journal of Air Waste and Management Association 51, 109-120.

Delfino, R.J., Becklake, M.R., Hanley, J., Singh, B., 1994. Estimation of unmeasured particulate air pollution data for an epidemiological study of daily respiratory morbidity. Environmental Research 67, 20-38.

Duclos, P., Sanderson, L.M., Lipsett, M., 1990. The 1987 forest fire disaster in California: assessment of emergency room visits. Archives of Environmental Health 45, 53-8.

Engel-Cox, J., Holloman, C., Coutant, B., Hoff, R., 2004. Qualitative and quantitative evaluation of MODIS satellite sensor data for regional and urban scale air quality, Atmospheric Environment 38, 2495-2509.

Falke, S.R., Husar, R.B., Schichtel, B.A., 2001. Fusion of SeaWiFS and TOMS satellite data with surface observations and topographic data during extreme aerosol events. Journal of the Air and Waste Management Association 51, 1579–1585.

Ferrare, R.A., Turner, D.D., Heilman, L.A., Dubovik, O., Feltz, W., 2001. Raman lidar measurements of the aerosol extinction-to-backscatter ratio over the Southern Great Plains. Journal of Geophysical Research 106, 20333-347.

Gumley, L., Descloitres, J., Schmaltz, J., 2003. Creating Reprojected True Color MODIS Images: A Tutorial. Accessed on May 5, 2005 at http://rapidfire.sci.gsfc.nasa.gov/faq/MODIS_True_Color.pdf.

Herr, L., 2003. Air quality impact quality impacts from the Megram and Onion Wildfires in Northern California. Available at http://www.ncuaqmd.org/documents/meagram.pdf. Accessed on May 1, 2005.

Husar, R.B., Tratt, D.M., Schichtel, B.A., Falke, S.R., Li, F., Jaffe, D., et al., 2001. The Asian dust events of April 1998. Journal of Geophysical Research-Atmospheres 106 (D16), 18317–18330.

Hutchinson, K.D., 2003. Applications of MODIS satellite data and products for monitoring air quality in the state of Texas. Atmospheric Environment 37, 2403–2412.

Kravchenko, A., Bullock, D.G., 1999. A comparative study of interpolation methods for mapping soil properties. Agronomy Journal 91, 393-400.

Kunii, O., Kanagawa, S., Yajima, I., Hisamatsu, Y., Yamamura, S., Amagai, T., Ismail I.T., 2002. The 1997 haze disaster in Indonesia: its air quality and health effects. Archives of Environmental Health 57, 16-22.

Lapen, D.R., Hayhoe, H.N., 2003. Spatial analysis of seasonal and annual temperature and precipitation normals in Southern Ontario, Canada. Journal of Great Lake Research 29, 529-544.

Lipsett, M., Hurley, S. , Ostra, B., 1997. Air pollution and emergency room visits for asthma in Santa Clara County, California. Environmental Health Perspectives 105, 216-222.

Mott, J.A., Meyer, P., Mannino, D., Redd, S.C, Smith, E.M., Gotway-Crawford, C., Chase, E., 2002. Wildland forest fire smoke: health effects and intervention evaluation, Hoopa, California, 1999. Western Journal of Medicine 176, 157-62.

Mueller, T.G., Mijatovic, B., Sears, B.G., Pusuluri, N., Stombaugh, T.S., 2004. Map quality for ordinary kriging and inverse distance weighted interpolation. Soil Science Society of America Journal 68, 2042–2047.

Nalder, I.A., Wein, R.W., 1998. Spatial interpolation of climatic normals: test of a new method in the Canadian boreal forest. Agriculture and Forest Meteorology 92, 211-225.

Ostro, B., Lipsett, M., Mann, J., Wiener, M., Selner, J., 1994. Indoor air pollution and asthma: Results from a panel study. American Journal of Respiratory and Critical Care Medicine 149, 1400-6.

Phuleria, H., Fine, P.M., Zhu, Y., Sioutas , C., 2005. Characterization of particulate matter and co-pollutants during the Fall 2003 southern California Fires. Journal of Geophysical Research, 110, D07S20, doi:10.1029/2004JD004626.

Pinto, J.P., Grant, L.D., 1999. Approaches to monitoring of air pollutants and evaluation of health impacts produced by biomass burning. In: Health Guidelines for Vegetation Fire Events - WHO/UNEP/WMO Background Papers pp. 149-185. World Health Organization.

Robin, L., 1996. Wood-burning stoves and lower respiratory illness in Navajo children. Pediatric Infectious Disease Journal 15, 859-865.

Voss, K.J., Welton, E. J., Quinn, P.K., Johnson, J., Thompson, A., Gordon, H.R., 2001. Lidar measurements during Aerosols99. Journal of Geophysical Research 106, 20821-20832.

Wang, J., Christopher, S.A., 2003. Intercomparison between satellite-derived aerosol optical thickness and PM2.5 mass: implications for air quality studies. Geophysical Research Letters 30, doi:10.1029/2003GL018174.

Ward, D.E., Hardy, C.C., 1991. Smoke emissions from wildland fires. Environmental International 17, 117-134.

Weber, D.D., Englund, E.J., 1992, Evaluation and comparison of spatial interpolators: Math. Geology 24, 381–391.

Zimmerman, D., Pavlik, C., Ruggles, A., Armstrong, M.P., 1999. An experimental comparison of ordinary and universal kriging and inverse distance weighting. Mathematical Geology 31, 375-390.

Table 1. Regression equations for filter-based data against TEOM or BAM data at co-located sites.

Pollutant	AQ Site	Instrument	N	Intercept	p(intercept)	Slope	p(slope)	R^2
PM_{10}	Los Angeles-North Main St.	BAM	19	-9.44	0.008	1.54	<.0001	0.94
PM_{10}	Riverside-Rubidoux	TEOM	47	-8.55	0.1142	1.03	<.0001	0.82
PM_{10}	Burbank	TEOM	16	-3.34	0.7144	1.35	<.0001	0.69
PM_{10}	North Long Beach	TEOM	26	1.46	0.6842	1.09	<.0001	0.79
$PM_{2.5}$	Riverside-Rubidoux	BAM	150	-2.30	0.0025	0.74	<.0001	0.93
$PM_{2.5}$	Burbank	BAM	30	-8.56	<.0001	0.85	<.0001	0.95
$PM_{2.5}$	Escondido	BAM	109	5.86	<.0001	0.48	<.0001	0.62
$PM_{2.5}$	Anaheim	BAM	142	-3.69	0.026	0.59	<.0001	0.63[a]

[a] This regression excluded two outliers.

Table 2. Regression equations for PM concentration against smoke and meteorology parameters (from August 1 to December 31, 2003; only those equations with $R^2 \geq 0.5$ are shown).

Pollutant	AQ Site	ASOS Site	Distance (km)	N	R^2	Intercept	ax	bx	Variable1	Variable2
PM_{10}	Lake Gregory			21	0.56	6.29	0.44	-6.94	Temperature	Wind speed
PM_{10}	Azusa			26	0.52	90.67	-27.02	52.35	Wind speed	Smoke
PM_{10}	Anaheim	Fullerton M Airport	8.3	153	0.82	25.06	4.62	115.62	B_{ext}_C	Smoke
PM_{10}	Riverside-Rubidoux	Riverside M Airport	5.8	152	0.59	29.64	14.20	63.91	B_{ext}_C	Smoke
PM_{10}	Norco	Chino Airport	8	139	0.54	-10.73	15.75	0.37	B_{ext}_C	Temperature
PM_{10}	Fontana	Ontario Airport	11.1	25	0.62	-31.82	14.35	0.94	B_{ext}	Temperature
PM_{10}	North Long Beach	Long Beach Daugherty Field	2.4	152	0.84	25.16	3.19	101.33	B_{ext}	Smoke
PM_{10}	Los Angeles-North Main St.	Los Angeles USC Camp	7.7	99	0.61	13.43	12.90	73.16	B_{ext}_C	Smoke
PM_{10}	Santa Clarita	Van Nuys Airport	20	26	0.59	-68.46	0.38	1.24	Relative humidity	Temperature
PM_{10}	Hawthorne	Hawthorne M Airport	3.3	121	0.67	17.02	5.35	51.13	B_{ext}	Smoke
PM_{10}	Escondido	Ramona Airport	18	25	0.73	-45.35	68.90	-0.73	B_{ext}	Relative humidity
PM_{10}	San Diego - Overland	San Diego Lindbergh Field	11.9	25	0.62	80.79	6.65	-0.85	B_{ext}	Relative humidity
PM_{10}	El Cajon	San Diego Montgomery Field	19	25	0.72	56.30	17.04	-0.72	B_{ext}	Relative humidity
PM_{10}	San Diego - 12th Ave.	San Diego Lindbergh Field	3.1	26	0.62	120.80	9.50	-1.26	B_{ext}	Relative humidity
$PM_{2.5}$	Anaheim	Fullerton M Airport	5.9	152	0.72	4.48	5.74	29.28	B_{ext}	Smoke
$PM_{2.5}$	Riverside-Rubidoux	Riverside M Airport	5.8	152	0.82	-5.59	11.55	16.69	B_{ext}	Smoke
$PM_{2.5}$	Riverside-Magnolia	Riverside M Airport	3.5	152	0.74	-19.03	11.57	0.20	B_{ext}	Temp
$PM_{2.5}$	Ontario	Chino Airport	7.2	152	0.74	2.13	7.83	6.77	B_{ext}	Smoke
$PM_{2.5}$	Fontana	Ontario Airport	11.1	43	0.86	-5.42	12.00	25.32	B_{ext}	Smoke
$PM_{2.5}$	North Long Beach	Long Beach Daugherty Field	2.4	127	0.82	0.28	8.51	35.79	B_{ext}	Smoke
$PM_{2.5}$	Reseda	Van Nuys Airport	4.2	122	0.60	4.85	6.99	-1.18	B_{ext}	Wind speed
$PM_{2.5}$	Lynwood	Hawthorne M Airport	11.4	49	0.75	11.05	7.11	-3.85	B_{ext}	Wind speed
$PM_{2.5}$	Pico Rivera	Fullerton M Airport	17	147	0.64	8.20	6.09	31.71	B_{ext}	Smoke
$PM_{2.5}$	Los Angeles-North Main St.	Los Angeles USC Camp	7.7	105	0.89	-0.56	8.23	36.10	B_{ext}	Smoke
$PM_{2.5}$	South Long Beach	Long Beach Daugherty Field	4.2	137	0.75	4.02	6.66	55.98	B_{ext}	Smoke
$PM_{2.5}$	Chula Vista	San Diego Brown Field	10	44	0.97	2.89	4.74	98.36	B_{ext}	Smoke
$PM_{2.5}$	Escondido	Ramona Airport	18	143	0.68	10.16	11.11	-0.24	B_{ext}	Temperature
$PM_{2.5}$	San Diego - Overland	San Diego Montgomery Field	2.5	45	0.98	0.56	5.20	68.51	B_{ext}	Smoke

FIGURE CAPTIONS

Figure 1. Flow-chart of the exposure assessment of particulate matters before, during and after the 2003 southern California wildfires

Figure 2. Air quality and ASOS stations overlaid with MODIS satellite image on 10/25/2003.

Figure 3. Measured PM concentrations under different smoke scenarios.

Figure 4. An example of a $PM_{2.5}$ pollution surface created by IDW and kriging for 10/2/2003.

Figure 5a. Polygons created for fire and smoke on 10/27/2003.

Figure 5b. Interpolated PM_{10} concentrations at zip-code centroids on 10/27/2003.

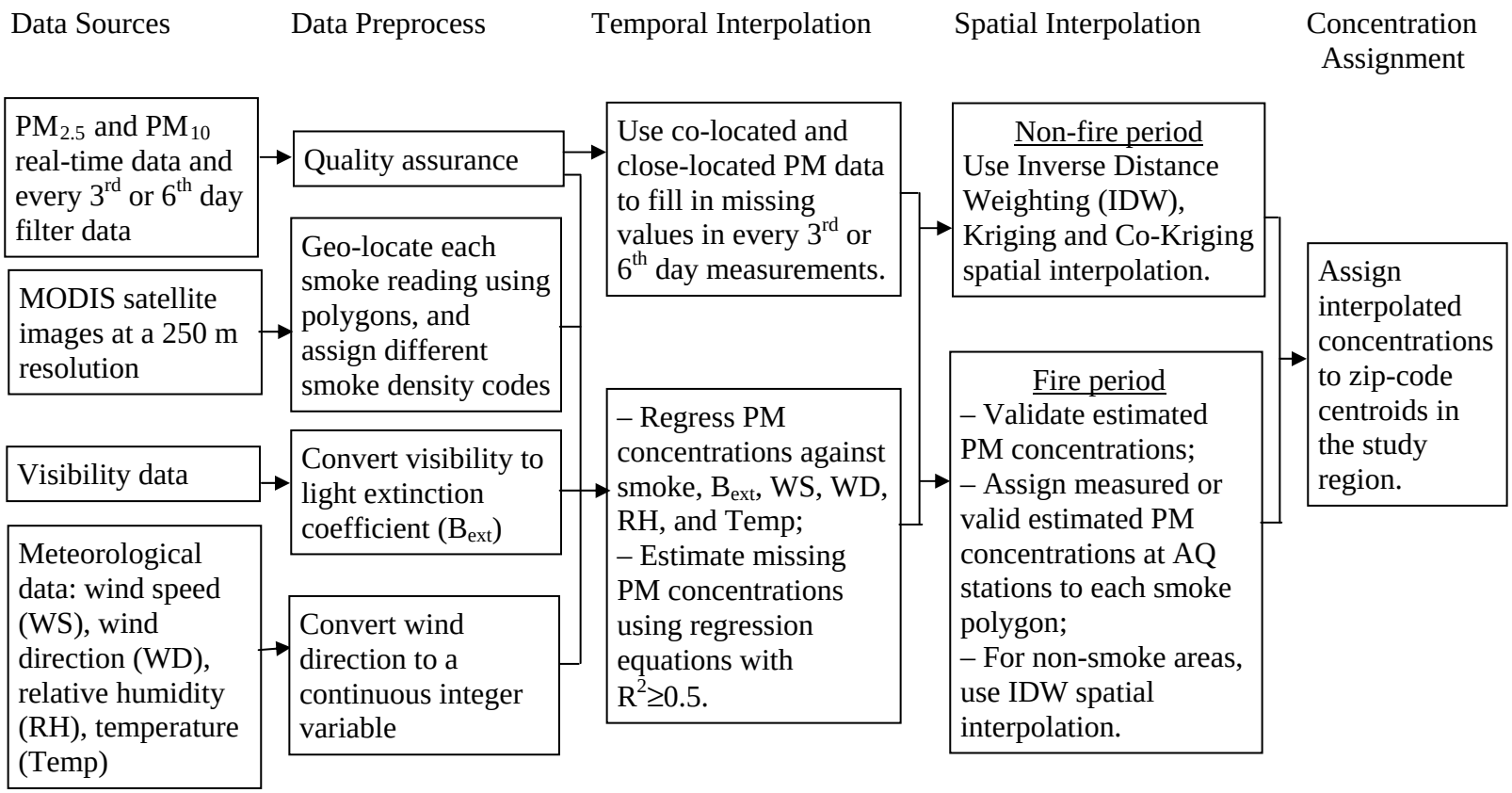

Figure 1. Flow-chart for the exposure assessment of particulate matter before, during and after the 2003 southern California wildfires.

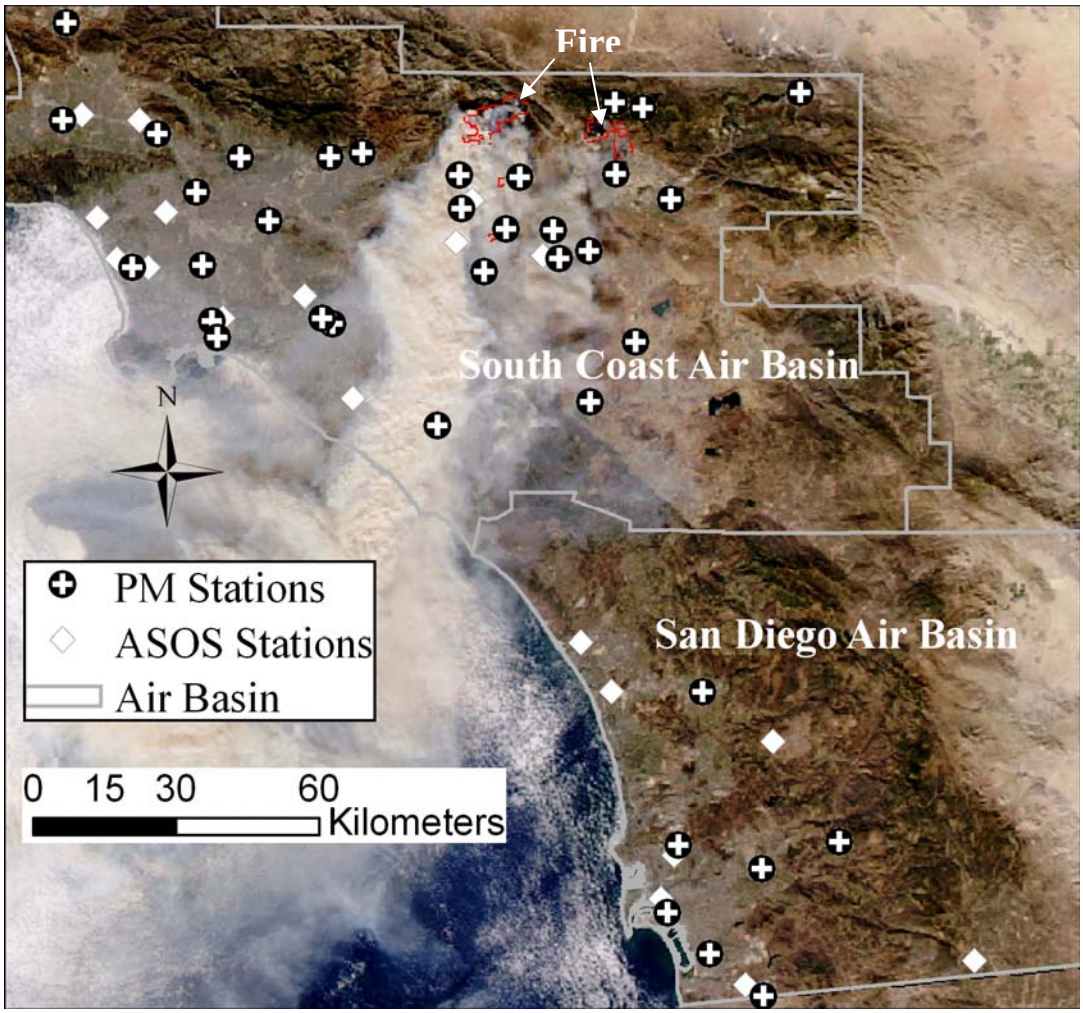

Figure 2. Air quality and ASOS stations overlaid with MODIS satellite image on 10/25/2003. The MODIS satellite data were obtained from the NASA's MODIS Rapid Response System (http://rapidfire.sci.gsfc.nasa.gov/gallery).

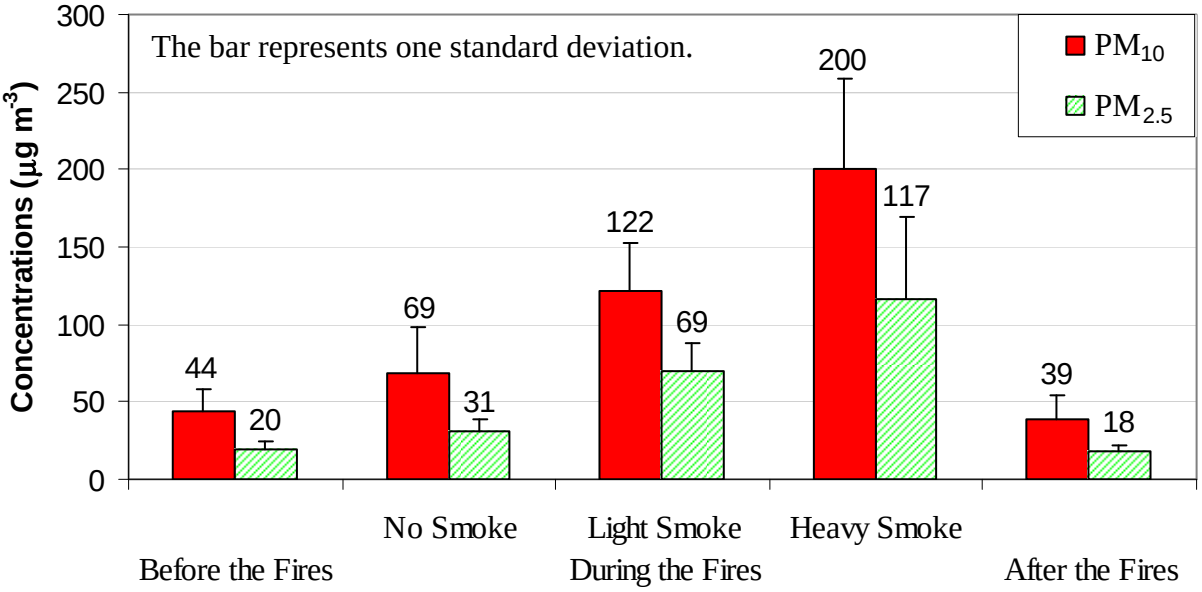

Figure 3. Measured PM concentrations under different smoke scenarios.

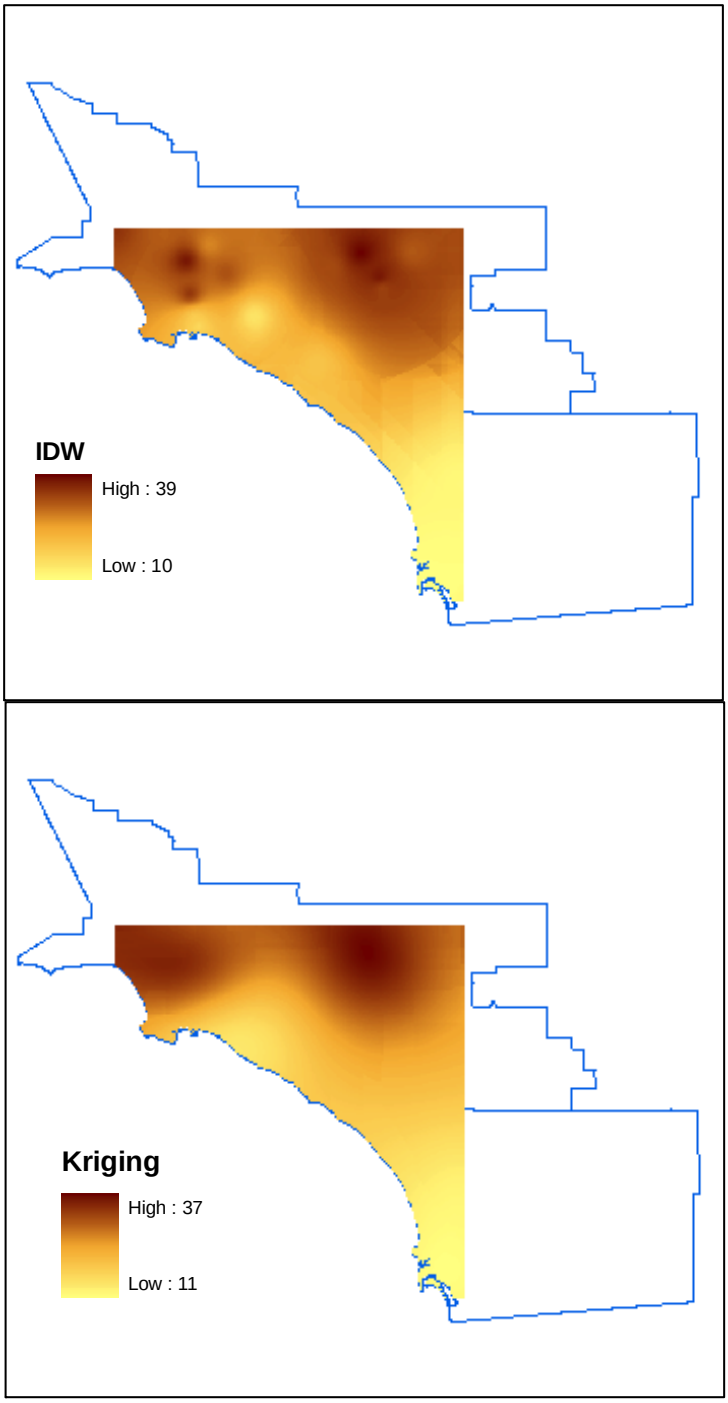

Figure 4. An example of a $PM_{2.5}$ pollution surface created by IDW and kriging for 10/2/2003.

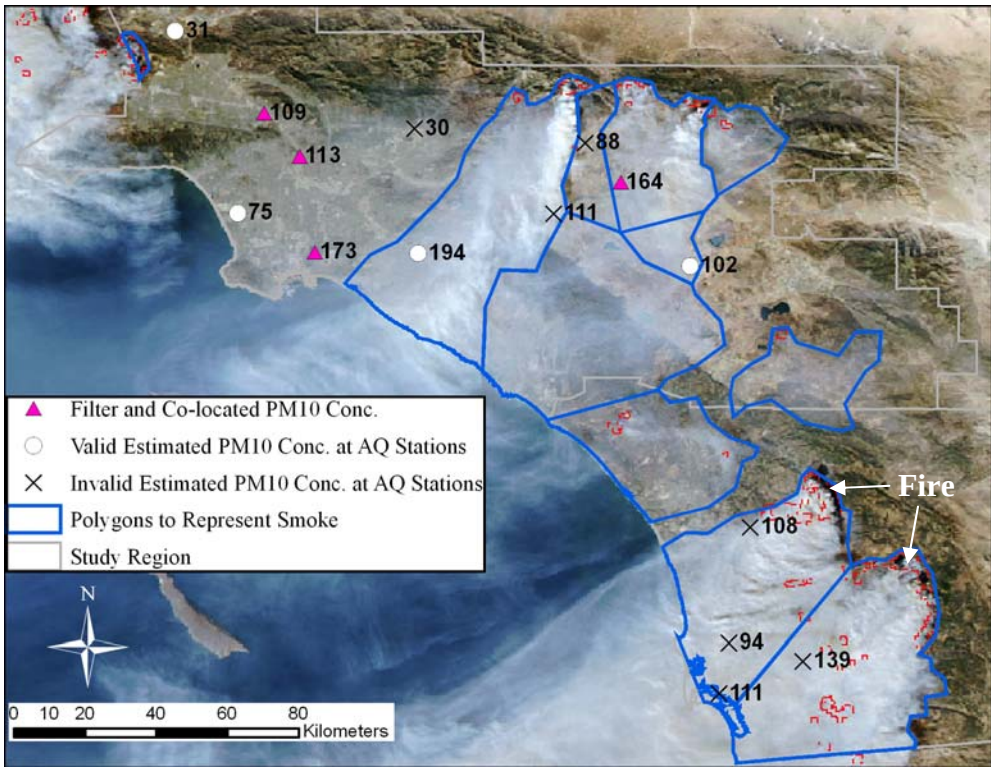

Figure 5a. Polygons created for fire and smoke on 10/27/2003.

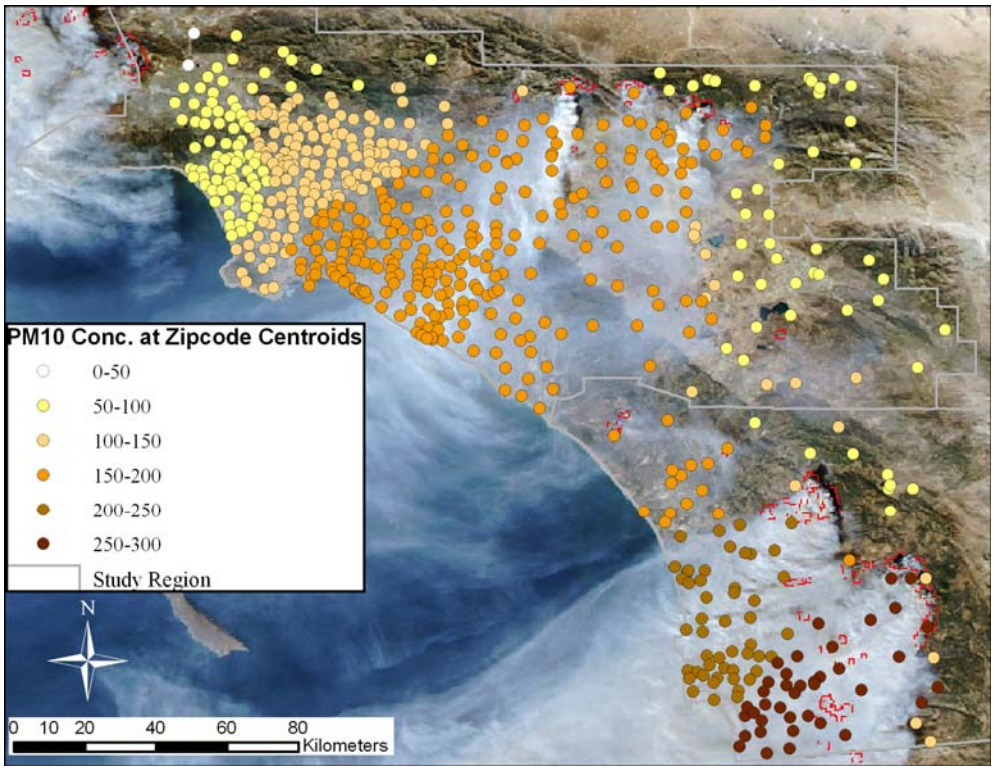

Figure 5b. Interpolated PM_{10} concentrations at zip-code centroids on 10/27/2003.